EMA-based Monitoring Method of Strengthened Beam-Column Joints

Constantin E. Chalioris
Democritus University of Thrace
chaliori@civil.duth.gr

Nikos A. Papadopoulos
Democritus University of Thrace
nikpapad@civil.duth.gr

George Sapidis
Democritus University of Thrace
gsapidis@civil.duth.gr

Maria C. Naoum
Democritus University of Thrace
mnaoum@civil.duth.gr

Emmanouil Golias
Democritus University of Thrace
egolias@civil.duth.gr

ABSTRACT

Reinforced concrete (RC) beam-column joints (BCJ) are crucial structural components, primarily during seismic excitations, so their structural health monitoring (SHM) is essential. Additionally, BCJ of existing old RC frame structures usually exhibits brittle behavior due to insufficient transverse reinforcement. To alter the brittle behavior of BCJ, an innovative reinforcing technique has been employed, accompanied by a real-time SHM system. Carbon fiber-reinforced polymer (C-FRP) rope as near surface-mounted (NSM) reinforcement has been utilized as external reinforcement of the column and the joint panel. The use of piezoelectric lead zirconate titanate (PZT) transducers for real-time SHM of BCJ sub-assemblages was investigated. Statistical damage indices, such as RMSD and MAPD, were employed to quantify the damage. Furthermore, an innovative approach based on hierarchical clustering was introduced. The experiment results revealed that the damage level of the reference and the retrofitted specimens were successfully diagnosed with PZT transducers.

Keywords

Structural Health Monitoring (SHM), Beam-Column Joint (BCJ), Carbon Fiber-Reinforced Polymer (C-FRP) Ropes, Hierarchical Clustering, Piezoelectric Lead Zirconate Titanate (PZT) Transducers.

INTRODUCTION

Reinforced concrete (RC) buildings constitute the majority of the structures dedicated to the dwelling. Several principal civil infrastructures worldwide are also constructed with RC, and frame RC structures have been proved as effective earthquake-resistant buildings. However, critical infrastructures (CI) are usually interconnected and, hence, interdependent. Consequently, their performance influences the performance of other CIs and depends on the other CIs' performance (Abdelgawad et al. 2019). Therefore, any reduction in the performance of RC could generate unpredictable consequences, especially when this coexisted with the subjection of unanticipated calamities such as seismic excitations (Mishra et al., 2019; Santarsiero et al., 2021). Under these circumstances, the induction of structural damage usually demonstrates the inadequacy of frame RC structure design codes and construction methods, depriving its strength and bearing capacity (Jagadale et al., 2020; Singh et al., 2021). Moreover, RC structural members develop a brittle failure behavior and insufficient hysteric energy consumption when a shear failure pre-occurs (Valença and Carmo, 2017).

Significant RC members with a crucial contribution to the stability of RC structures, particularly after an

earthquake occurrence, are the Beam-column joints (BCJ). BCJs mainly suffer from the shear failure of beams and joints under the formation of plastic hinges, mostly appearing in soft story cases. Failures in the BCJ can be ascribed to agents like material weakness, lack of ductility, and insufficient shear reinforcement. Therefore, determining the failure modes and savvying the mechanical behavior of BCJ by assessing the joint shear capacity is pivotal. Furthermore, applicable methods for evaluating the strength of BCJ and determining the efficacy of implemented strengthening methods could be aspects of the resilience of RC structures.

In the last decades, fiber-reinforced polymers (FRP) composite materials and fiber-reinforced concrete heavily substituted the conventional steel bars, which were mainly used in the past for the strengthening of inadequate RC structural members subjected to seismic or cyclic loading (Karayannis et al., 2022; Karayannis and Sirkelis, 2008; Tafsirojjaman et al., 2021; Tsonos, 2009; Tsonos, 2014; Wang et al., 2022; Wang et al., 2022). Some applications include FRP sheets, FRP reinforcing bars with carbon fibers, and carbon FRP rope (C. Chalioris et al., 2018; Golias et al., 2021; Karayannis et al., 2022). Especially the latter constitutes a newly emerging technique for strengthening RC BCJs, due to its merits of the fast and easy retrofitting application.

Premature and precise evaluation of structural deterioration can significantly prevent unpleasant casualties and preserve repair costs to an affordable extent. SHM systems are employed to monitor the actual operation status of critical infrastructure continuously (Psathas et al. 2022). However, traditional SHM methods are costly and scant, particularly for inaccessible structural members, indicating the demand for innovative, next-generation monitoring technologies research (Gandhi et al. 2018). Therefore, from the perspective of structural safety, an established technique suitable for monitoring critical RC members is undoubtedly research of high priority and significance (Voutetaki et al. 2021, Voutetaki et al. 2022, Karayannis et al., 2022).

The electro-mechanical admittance (EMA) method effectively addresses this problem via early real-time cracking detection measuring structural vibrations. The application of the EMA method heavily relies on the advantages of smart piezoelectric materials such as piezoelectric lead zirconate titanate (PZT) patches. Their low energy consumption, low cost, ease of applicability, small size, portability, and simultaneously double functional operation as sensors and actuators are some desirable features in SHM applications (Chen et al., 2019; Pham et al., 2021). The EMA method employs the principles of the electro-mechanical coupling effect to detect abnormalities in the structural integrity of the host structure.

Recent studies have indicated that implementing a PZT network in regions of potential damage development enhances the efficiency and the accuracy of the SHM methods to detect damage levels providing a reliable diagnosis (C. E. Chalioris et al., 2015; Jiang et al., 2016; Voutetaki et al., 2016; Yan et al., 2009; Zhang et al., 2018, Zapris et al. 2023). In particular, a clustering approach introduced by Perera et al. (Perera et al., 2019) and Sevillano et al. (Sevillano et al., 2016) upgraded PZT-based SHM that satisfactorily evaluates several measurements acquired from the PZT transducers and diagnoses damage in RC members strengthened with FRP materials.

This work examines the application of externally mounted FRP ropes as a near-surface mounted (NSM) reinforcement to strengthen the columns and the joint panel of two real-scale BCJ sub-assemblages. Moreover, PZT transducers are employed to investigate the efficiency of the proposed strengthening technique's efficacy. Further, the PZT transducers' effectiveness in diagnosing the developed damage in the BCJ specimens under the cyclic loading subjection has also been investigated. Any acquired difference in the voltage response captured by the advanced wireless monitoring system is depicted in the PZT patch's electro-mechanical signature. Further, any change to the depicted electro-mechanical signature from the pristine to any sequence state is related to an abnormality in the PZT patch's contiguity.

Damage diagnosis using EMA-based PZT-enabled SHM techniques in RC structural members subjected to seismic or quasi-static loading has not been deeply investigated. However, earthquake damages increase structural vulnerability.

Additionally, the efficacy of the retrofitting technique was investigated by applying multiple types of transducers, such as:

- String linear variable displacement transducers (SLVDTs) mounted on the diagonals of the BCJs measuring the shear deformations of the joint panel
- PZT sensors on the C-FRP ropes and the concrete
- Laser Displacement Transducers (LDTs)

The application of PZT transducers in C-FRP ropes for continuous monitoring and the prompt diagnosis of fatal

debonding of the composite reinforcement or diagonal shear cracking of joint concrete has not been examined in depth. Further, the investigation of the efficacy of this strengthening technique by combining traditional displacement transducers and PZT transducers has not been extensively investigated.

A mass casualty incident (MCI) is defined as an "event which generates more patients at one time than locally available resources can manage using routine procedures" (Berndt et al., 2018). Thus, the authorities of potentially affected regions need to prepare themselves. Early warning, risk, and crisis management systems can provide these authorities with the necessary methods for decision support (Moßgraber et al., 2018).

Therefore, the proposed approach allows for intelligent monitoring of critical members of structures and infrastructures under crisis conditions such as earthquake excitations, terrorist or accidental explosions, aging, and other natural hazards. Furthermore, by implementing the proposed SHM technique, crucial information could be obtained about the health integrity of the examined structural member before, during, or after a disaster or crisis event, providing essential data to the practitioners to design an operational plan for crisis management either remotely or in situ. Thus, combining a recently developed strengthening technique using C-FRR ropes and a SHM technique for monitoring the RC structure and the retrofitted section meet the demand for resilient structures and, thereby, resilient societies, maintaining essential functions under stressful and harsh conditions (Comes et.al., 2013).

Furthermore, for suddenly developed occurrences with significant damages, the proposed SHM technique could primarily help to evaluate the accessibility of the defective area. Further, it could assist in a targeted repairing or retrofitting plan in long-developed incidents such as aging or fatigue actions, and even worst, to forbid the operation or to evacuate the monitored infrastructure. In addition, this study aims to emerge that the proposed SHM technique can provide real-time, continuous inspection and in-situ measurement for far-field damage diagnosis and prompt warning of the impending failure in real-life RC structures.

Table 1. A list of Abbreviations

RC	*Reinforced Concrete*	**FRP**	*Fiber-reinforced Polymers*
BCJ	*Beam-Column Joints*	**EMA**	*Electro-mechanical Admittance*
SHM	*Structural Health Monitoring*	**SLVDT**	*String Linear Variable Displacement Transducer*
C-FRP	*Carbon Fiber-reinforced Polymer*	**LDT**	*Laser Displacement Transducer*
NSM	*Near Surface-mounted*	**MCI**	*Mass Casualty Incident*
PZT	*Piezoelectric lead Zirconate Titanate*	**HCA**	*Hierarchical Clustering Approach*
RMSD	*Root Mean Square Deviation*	**CCC**	*Cophenetic Correlation Coefficient*
MAPD	*Mean Absolute Percentage Deviation*	**SD**	*Story Drift*
CI	*Critical Infrastructures*		

MATERIALS AND METHONDS

Design of the BCJ specimens

The geometrical characteristics, the manufacturing materials, and the steel reinforcements details of the examined sub-assemblages represented the design of an ordinary RC frame, as shown in Figure 1. For the two examined specimens (initial and retrofitted), both column's and beam's cross-sectional dimensions were 350/250 with a length of 3.0 m and 1.875 m, respectively.

This test project aimed to examine the efficacy of the C-FRP ropes' implementation as additional strengthening longitudinal and transverse reinforcement of the column and shear reinforcement of the joint panel. The C-FRP ropes were diagonally placed on the two sides of the BCJ sub-assemblage, forming an (X) shape on both sides of the joint panels. Specimen JC0F2X2C has been externally retrofitted in this scope with C-FRP ropes under the NSM applied technique, enhancing the column's flexural resistance placed as longitudinal reinforcement along its height. Additionally, three C-FRP ropes were placed as closed stirrups in the critical column-joint regions, strengthening the transverse shear resistance of the column. Furthermore, four C-FRP ropes were diagonally and symmetrically wrapped on the joint panel (two on each side), aggrandizing the shear capacity of the joint. The applied retrofitting scheme is displayed in Figure 2.

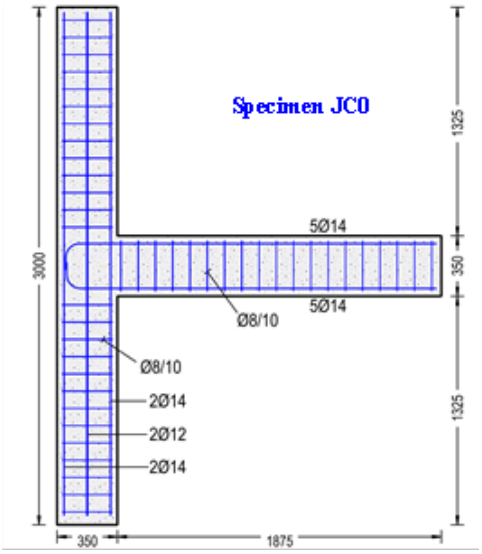

Figure 1. Geometric and reinforcement details of the ordinary RC

Applying the proposed technique inserts some degrees of difficulty and embeds processes that must be diligently performed. The method of the NSM technique is gleaned from the below steps:

1. Engraving and carving of the channels (20-25 mm depth) for the insertion of the ropes and formation of the U-shaped notches; special attention should be paid to the protection of the existing conventional steel rebars and reinforcing stirrups from damaging them during the incising works;
2. Removing the dust inside the carved channels with compressed air;
3. Smoothing out and rounding to a radius of 20 mm the corners where the rope needs to be revolved
4. Impregnation of the rope to epoxy resin according to the manufacturer's TDS;
5. Insertion and gliding of the impregnated C-FRP ropes into the formed channels; Forming of the anchorage of C-FRP ropes;
6. Channel's repletion with an epoxy resin to enhance coherence among the inserted materials and the anchorage of the rope. (Golias et al., 2021; Karayannis et al., 2022).

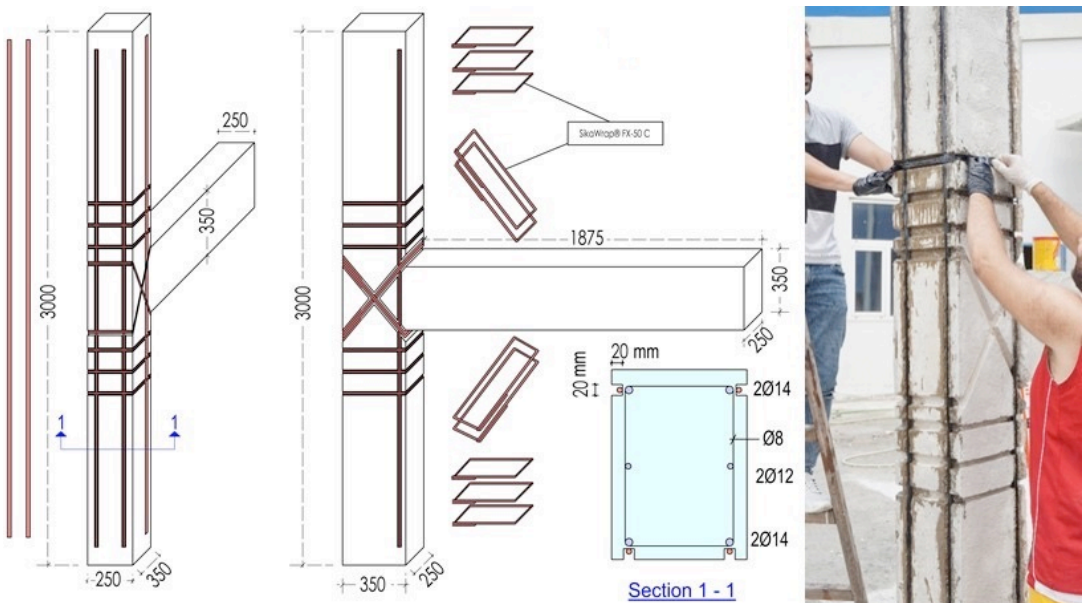

Figure 2. Dimensions and strengthening scheme applied on specimen JC0F2X2C

Compression tests were performed in six standard cylinders to evaluate the concrete's compressive strength. In Table 2, the properties of the applied materials are presented.

Table 2. Material properties

Concrete	*Compressive strength*	34 MPa
Reinforcement steel bars	*Yield strength*	550 MPa
C-FRP ropes	*Tensile strength*	4000 MPa
	Modulus elasticity	240 GPa

Examination of the expected damage

The failure mode of the BCJ sub-assemblages was studied based on the well-established model developed by Tsonos (Tsonos, 2019). According to this model, the ultimate shear stress τ_{ult} (Equation 1) of the joint and the factor γ_{ult} (Equation 2).

$$\gamma_{ult} = \tau_{ult}/\sqrt{f_{cm}} \tag{1}$$

are first defined and then collated to the developing shear stress τ_{cal} and the related factor γ_{cal}.

$$\gamma_{cal} = \tau_{cal}/\sqrt{f_{cm}} \tag{2}$$

From this comparison, it was derived that the anticipated damage and expected critical cracking would be localized in the joint body, which was finally verified by the cyclic loading tests.

Test Setup

The tests were performed in a strong and rigid RC floor wall. Firstly, a 90 degrees rotation was applied to the tested specimens so that the column followed the horizontal direction while the beam reversed to the vertical one. The column of the RC BCJ specimens was sufficiently anchored to the floor through a sandwich metal plate mechanism also fixed with bolts and nuts to avoid the specimen's slippage. Furthermore, a servo-controlled hydraulic actuator settled to the rigid wall of the testing area and imposed the load on the end of the beam.

Under this formation, a permanent axial compressive load equal to $N_c = 5\%\ A_c\ f_{cm}$ was transferred in the sub-assemblage column for the whole experimental duration. The test setup and the imposed cyclic loading sequence are shown in Figure 3. Both specimens were subjected to the same loading history of cyclic deformations displayed in terms of story drift.

The sequence of the cyclic loading constituted eight steps with imposed deformations: ±8.50 mm, ±12.75 mm, ±17.00 mm, ±25.50 mm, ±34.00 mm, ±51.00 mm, ±68.00 mm, and ±85.00 mm that correspond to SD: 0.50%, 0.75%, 1.00%, 1.50%, 2.00%, 3.00%, 4.00%, and 5.00%, respectively. Each loading step included three full loading cycles, as displayed in Figure 3.

The recorded characteristic responses of the tested sub-assemblages were acquired using the below instrumental equipment: a) the imposed displacement near the beam's free end was measured with laser displacement transducers (LDTs), b) the imposed loading near the beam's free end was measured with a load cell, c) PZT transducers applied on the ropes and the concrete for diagnosing the damage level/severity.

Diagonal SLVDTs and measurement of shear deformations

A common phenomenon presented in the BCJs' panels of the multi-story RC frame structure is the development of shear deformatted areas under the subjection of seismic excitations. This phenomenon composes a strong indication of potential cracking and damage level. Additionally, the determination of shear deformations can be constituted as a straightforward and efficient process to evaluate the efficacy of the applied strengthening technique to enhance the seismic performance of the BCJ.

In this study, two diagonally mounted on the joint panel SLVDTs were used to measure the developed shear deformations under the subjection of cyclic testing. Thus, the SLVDTs can measure both the elongation and the shortening of the diagonals of the joint panel. Therefore, according to the acquired measurements, there are two ways of calculating shear deformations for each abovementioned condition.

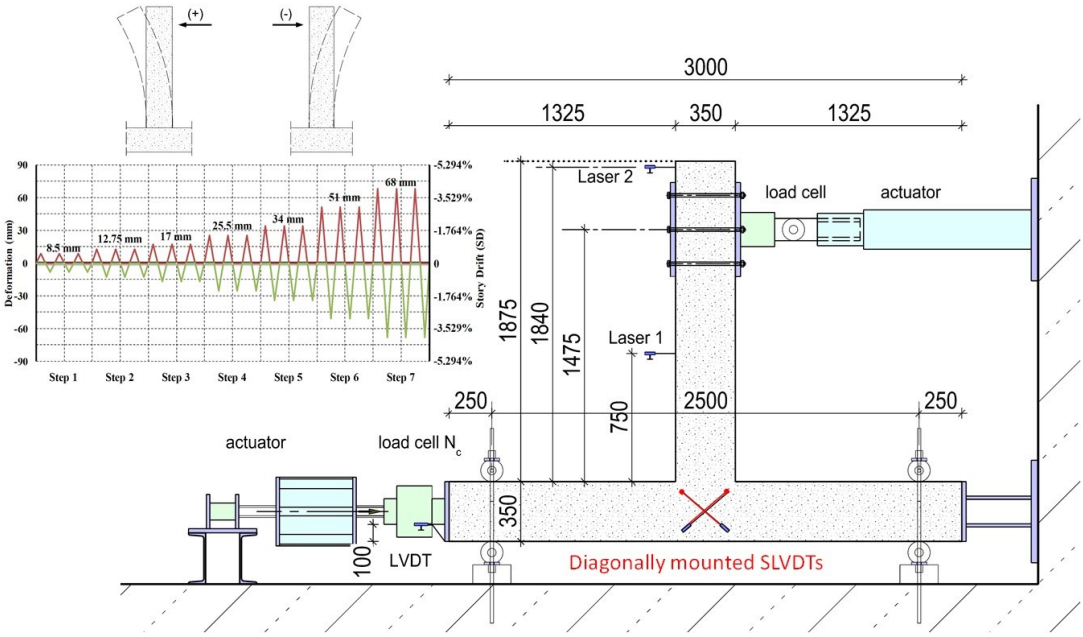

Figure 3. Experimental setup and loading sequence

From the elongation Δ_1 of diagonal AC shown in figure 4a, the shear deformation can be calculated as $\gamma_1 = \delta/h_1$; where $h_1 = L_1 cos\varphi_1$ and L_1 is the length of the diagonal SLVDT1. Further from the triangle CC'C" it is determined that: $\delta = \Delta_1/\cos(90-\varphi_1) = \Delta_1/\sin\varphi_1$ and $\gamma_1 = (\Delta_1/\sin\varphi_1)/(L_1\cos\varphi_1) = \Delta_1/(L_1 \sin\varphi_1 \cos\varphi_1) = 2\Delta_1/(L_1 \sin 2\varphi_1)$.

Similarly, from the shortening Δ_2 of the diagonal BD and the triangle BB'B" the shear deformation γ_2 is deduced that $\gamma_2 = 2\Delta_2/(L_2 sin2\varphi_2)$.

Since the joint panel has a symmetric shape, it can be assumed that L_1 and L_2 are approximately equal ($L_1 \approx L_2$) and $\varphi_1 \approx \varphi_2$.

Therewithal, let L = L1 = L2 and φ = φ1 = φ2, and thereof the average shear deformation γ_{avg} (Equation 3) is estimated as:

$$\gamma_{avg} = \frac{\gamma_1+\gamma_2}{2} \rightarrow \gamma_{avg} = \frac{\Delta_1+\Delta_2}{Lsin2\varphi} \quad (3)$$

The diagonal SLVDTs mounted on specimen JC0 and on specimen JC0F2X2C are shown in Figures 5 and 6, respectively.

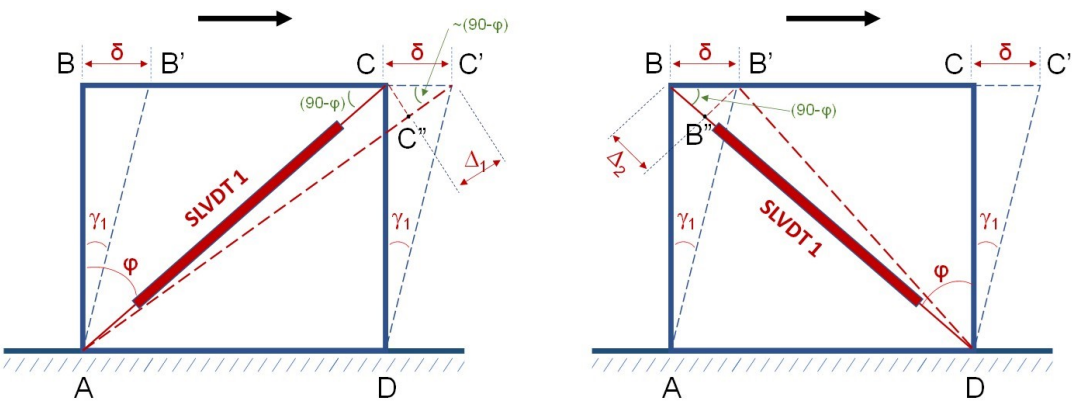

Figure 4. Scheme for elongation (a) and shortening (b) of SLVDTs mounted in the joint panel

Electro-mechanical admittance (EMA) method

The electro-mechanical admittance (EMA) method utilizes the merits of employed PZT transducers and their predominant feature of application based on the advantages of the piezoelectric phenomenon. The subjection of mechanical stress generates an electric charge; inversely, an applied electric field generates mechanical vibrations. Hence, presuming upon the piezoelectric phenomenon through the operation and the emitted pulses of mounted or embedded PZT transducers to a host RC member, any shifting to the electro-mechanical admittance (or its inverse impedance) is also displayed in the acquired electrical signal of the PZT. Additionally, the electro-mechanical signals are obtained in terms of the exciting frequency range, constituting the electro-mechanical signature of the instated PZT transducer. Thus, any observed change to the electro-mechanical signature of the PZT transducer includes a possible indication of potential structural anomalies existing in the effective monitoring region in the contiguity of the transducer. The structural abnormalities could be composed of concrete cracking or/and steel yielding.

Hence, the discrepancies observed in the frequency response curves at each loading step represent the internal or external damage state that occurred in the joint region until that loading step, reflecting the damage state of the material in the contiguity of the PZT.

In this experimental study, the applied method for diagnosing the development of potential abnormalities consists of the employment of the PZT transducers operating concurrently as actuators, excited with a 2.5 V harmonic voltage in terms of a frequency range between 10 to 250 kHz per step of 1 kHz and as sensors, acquiring the extracted electro-mechanical signals. The amplified Voltage signal was excited through the PZT patches, and the electro-mechanical signatures were obtained through a custom-made wireless device with the abbreviated notation WiAMS. This device can execute many calculations in a short time frame, performing high-power processing and being remotely administered.

The primary EMA measurements were extracted in the examined member's pristine condition, considered a healthy baseline state. Hence, the level of structural integrity was evaluated through comparisons of the results at different potential damage states and determined through statistical indices.

Each loading step brought about changes in the structure resulting in changes in the position and the shape of the recorded curve compared to the one as recorded at the beginning of the loading procedure (healthy condition). Thereupon, it may be assumed that the frequency response magnitude changes at the end of each loading step compared to the baseline one, which corresponds to the structure without any damage. This way, the discrepancies observed in the frequency response curves at each loading step represent the level of internal or external damage that occurred in the joint area until that loading step, reflecting the damage state of the material in the vicinity of the PZT.

Installation of PZT transducers

The identical PZT transducers with dimensions 20 x 20 x 5 mm were installed in both specimens. Their sign mark was PIC151, manufactured by PI Ceramics company. Thus, three PZT patches have been externally mounted with an epoxy resin on the examined BCJs. Initially, in JC0, the PZT patches' positioning was selected in such a way as to monitor the joint panel of the BCJ specimen (Figure 5). Hence, the PZTs were surficial epoxy-bonded on the concrete in the diagonal of the joint panel. Further, in JC0F2X2C, two PZT patches were placed on the diagonally mounted C-FRP ropes, to monitor the performance of the proposed retrofitting technique (Figure 6). Additionally, one PZT patch was bonded on the exterior concrete surface of the joint panel.

Damage Quantification Method

The damage quantification process attempts to demonstrate the diagnosis of the damage and determine its qualities, including the location and range of the crack/cracks. Additionally, the process is oriented to the instrumental evaluation and quantification of the damage's severity. The acquired measurements are analyzed and evaluated through statistical indices in this scope. The elaboration of the electro-mechanical measurements through statistical indices could be a valued tool in modifying the alterations of EMA measurements between the pristine condition and any subsequent one to damage index metrics.

Plenty of indices are proposed to the extent of literature, with the most commonly used being the following:

1. RMSD: Root Mean Square Deviation;
2. MAPD: Mean Absolute Percentage Deviation;
3. CC: Coefficient of Correlation;

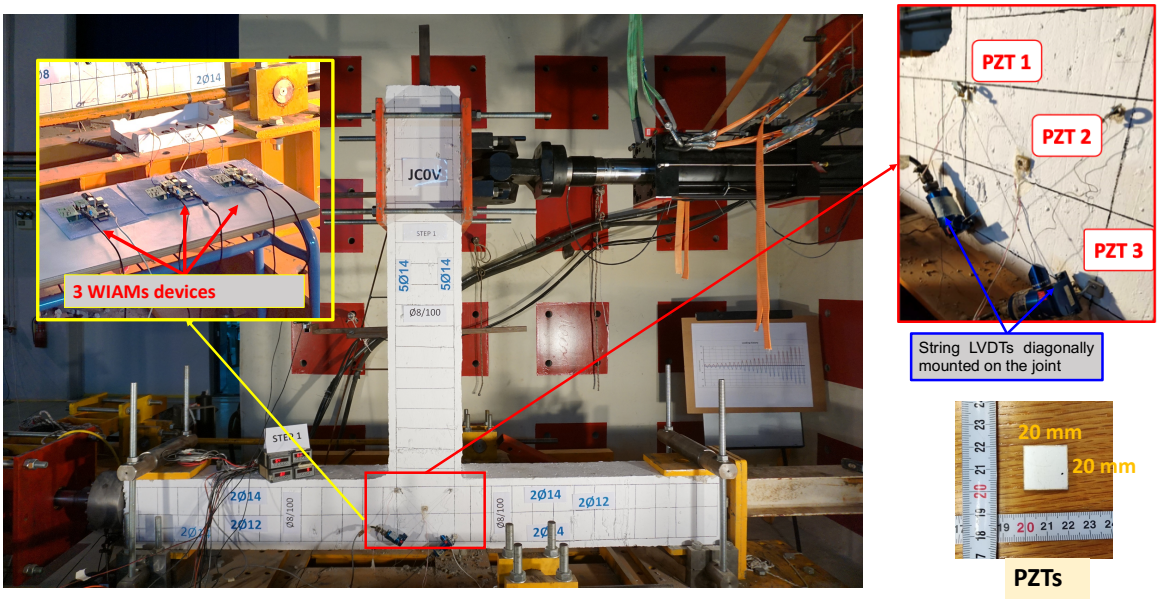

Figure 5. Measurement devices and PZT attached to specimen JC0

Figure 6. Measurement devices and PZT attached to specimen JC0F2X2C

In this study, the commonly used damage indices RMSD and MAPD were primarily applied for the statistical analysis of the EMA signatures. Therefore, the expression of the traditional RMSD and MAPD indices are also presented below in Equations 4 and 5, respectively:

$$\mathrm{RMSD} = \sqrt{\frac{\sum_{r=1}^{n}\left(\left|V_p(f_r)\right|_D - \left|V_p(f_r)\right|_0\right)^2}{\sum_{r=1}^{n}\left(\left|V_p(f_r)\right|_0\right)^2}} \tag{4}$$

$$\mathrm{MAPD} = \frac{1}{n}\sum_{r=1}^{n}\frac{\left|\left|V_p(f_r)_D - V_p(f_r)_0\right|\right|}{V_p(f_r)_0} \tag{5}$$

Where $\left|V_p(f_r)\right|_0$ is the absolute value of the voltage output signal extracted from the PZT at the Healthy pristine state of the specimen, $\left|V_p(f_r)\right|_D$ is the absolute value of the corresponding voltage output signal as measured from the same PZT at damage level D.

The pluralism of the applied indices demands an increased workload for collecting and editing the inserted data correctly and an increased workload for observing and analyzing the results among the different indices. However, employing multiple indices for the statistical analysis of damage detection could be a closer step to verging a complete damage quantification methodology.

Although the fact that the commonly used statistical indices show satisfying performance and good efficiency in the identification of damage's existence, there are still some deficiencies that have not been overcome in concrete applications due to the complicated feature of the material and the impact of different phenomena acting individually, together or consecutively. These cases decrease the reliability of statistical indices' efficacy for different cracking severity; the damage indices could have the same value and vice versa due to their scalar nature. Therefore, an efficient approach to solving the above deficiency is the combination of different damage indices or, even better, combining various data analysis methods.

For this purpose, the Hierarchical Clustering Approach (HCA) has been implemented in this study. In general, clustering is an unsupervised learning algorithm that can group observations concerning the degree of their similarity (Tsintotas et al., 2018, 2022). The fundamental hypothesis in the clustering approach for PZT applications is that the acquired measurements for the same PZT transducer at different loading steps are expected to demonstrate a similar behavior except if deformation occurs, which should be correlated with damage's existence (Perera et al., 2019).

In HCA, each measurement is considered and inserted as a single group. After that, employing a reiterative process, the dendrograms with similar observations are merged into a new cluster. Thus, an agglomerative methodology is structured. Finally, a dendrogram is used to better visualize different stages of clustering, classifying the dissimilarity among the formed groups. Additionally, the number of the total initial clusters is always between 1 and n, where n is the number of the inserted measurements. The decision about the final number of clusters depends on the data analyst's desire, experience, and training to set and combine the efficient number of clusters.

The main principles of the hierarchical algorithm are summarized in the below steps:

- Insertion of all the desired measurements into the system;
- Allocation of the measurements to a cluster. The algorithm starts with all the measurements, initially consist a cluster;
- Creating the first clusters by merging some single measurements with best-fit similarity;
- Re-computation of the distances between the newly formed clusters and the initial ones;
- The algorithm stops whenever all the measurements are assigned to a cluster or until the formation of the clusters' designed number.

Except for the above steps, two more coefficients, such as distance metric and linkage criterion, must be defined. The linkage criterion verifies or not the fidelity of the represented clustering and is a measure of how faithfully a dendrogram preserves the pairwise distances (distance matrix) between the original unmodeled data points.

This study selects the Euclidean distance metrics (Equation 6) and the cophenetic correlation coefficient (Equation 7) with moderate performance.

$$d_{st} = \sqrt{\sum_{i=1}^{n}(x_s - x_t)^2} \tag{6}$$

Where:

d_{st} is the Euclidean distance between each pair of observations, s and t,

x_s and x_t denote the vectors (1-by-n) of impedance signature of PZT in different conditions.

$$CCC = \frac{\sum_{s<t}(d_{st}-\bar{d})\left(d_{st}^{coph}-\bar{d}^{coph}\right)}{\sqrt{\sum_{s<t}(d_{st}-\bar{d})^2 \sum_{s<t}\left(d_{st}^{coph}-\bar{d}^{coph}\right)^2}} \tag{7}$$

Where CCC denotes the cophenetic correlation coefficient, while d_{st}^{coph} corresponds to cophenetic distances, which represent the dissimilarity of the cluster where s and t merged first.

TEST RESULTS AND DISCUSSION

Hysteretic curves and dissipated energy

Figure 7 presents the hysteretic responses of the two examined BCJs in terms of the applied load versus deformation curves. From the hysteretic curves of specimen JC0, it can be noticed that the maximum loads of hysteretic cycles at the 6th and 7th loading steps are notably lower than the maximum loads of the previous step (5th step). In Figure 8, a closer individual view of the hysteretic response curves sequence shows that the maximum load for specimen JC0 decreases abruptly between the 1st positive and the 1st negative cycle loading at the 6th loading step for Story Drift (SD) 3 %. Similarly, the corresponding maximum load of specimen JC0F2X2C decreases between the 1st positive and the 1st negative cycle loading for SD 3%, which is reflected at the 6th loading step. Thereby, it may be assumed that significant damage occurred at these steps. Furthermore, from the 1st loading step, specimen JC0F2X2C shows greater maximum loads of hysteretic response. Further, the specimen showed a prolonged performance, enduring up to the 8th loading step, which is owed to the contribution of the retrofitting technique.

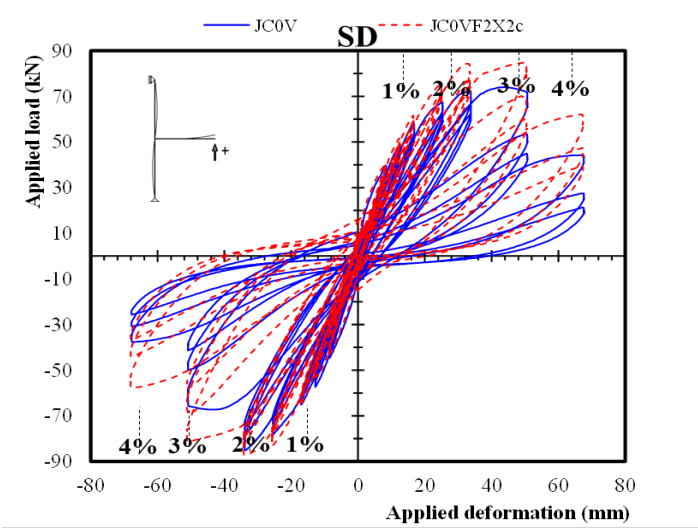

Figure 7. Hysteretic performance of specimens JC0 and JC0F2X2C

Furthermore, Figure 9 displays the dissipated energy values of the examined specimens in terms of the area of the hysteretic cycles per loading steps 1st, 2nd, and 3rd. This figure shows that the dissipated energy values of specimen JC0F2X2C with the C-FRP ropes are in all cycles higher than specimen JC0. The dissipated energy curves verify the assumption that at 6th loading step, significant damage has occurred in specimen JC0, as energy consumption capability has been significantly reduced.

In addition, a visual evaluation of the damage state of both specimens is displayed in Figures 10a and 10b. The assessment is addressed by comparing the corresponding condition of the specimens at the end of the testing procedure (end of load steps 7 and 8, respectively). From the cracking pattern of the BCJs presented in these figures, critical and significant cracks and extensive joint deterioration have been occurred in the joint body of specimen JC0, while in specimen JC0F2X2C the cracks and the concrete damages remained controlled, although the specimen completed one more cyclic loading step and performed higher value of deformation. Thus, it is consequentially demonstrated that the implemented strengthening technique has beneficially meliorated the seismic capacity of the BCJ specimen and maintained the body uncollapsed.

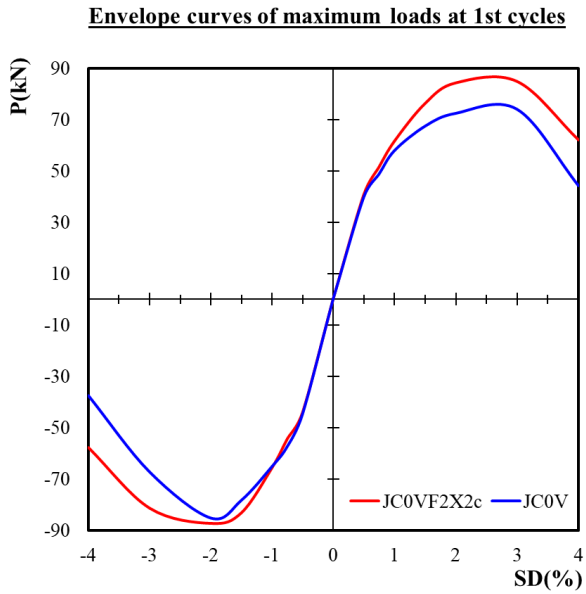

Figure 8. Envelopes of the 1st cycle of the hysteretic behaviour of the specimens JC0 and JC0F2X2C

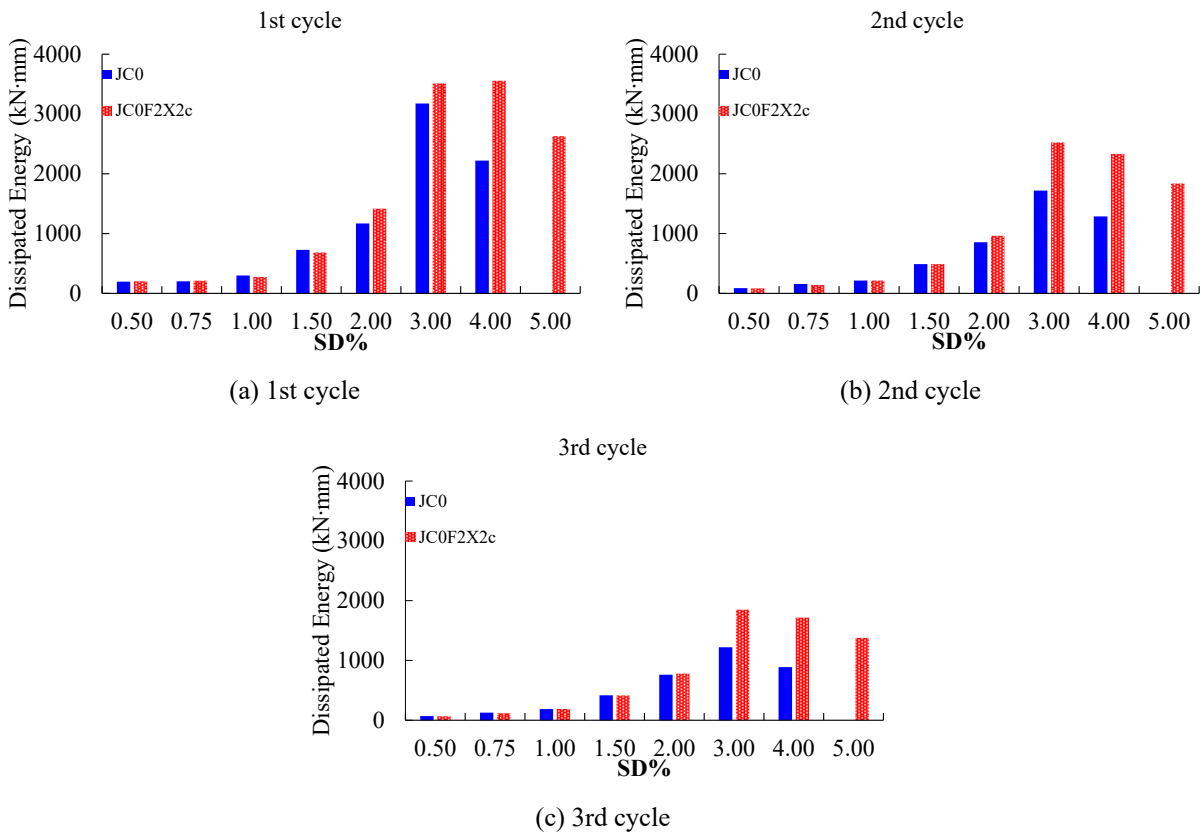

Figure 9. Dissipated energy of the two specimens in terms of the area of the hysteretic cycles

(a) JCOV (b) JC0F2X2C

Figure 10. Comparison of damage intensity between the two specimens after the final loading step

Shear deformations of the joint panel

Figure 11 presents the curves of the maximum absolute average values of the shear deformations of the joint panel γ_{avg} (in rad) versus the SD of the tested specimens. The shear deformations' values were measured through the diagonal SLVDTs and estimated through equations (1)-(4).

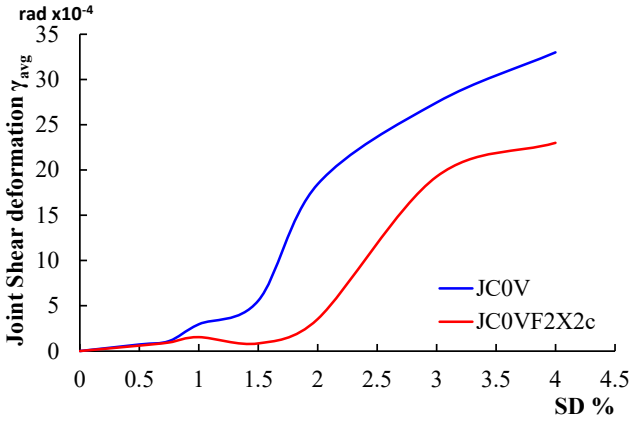

Figure 11. Shear deformations from the SLVDTs of the joint of the tested specimens JC0 and JC0F2X2C

As extracted from the curves of Figure 11, specimen JC0 demonstrates greater values of shear deformation than specimen JC0F2X2C. The latter is ascribed to the beneficial impact of the diagonal application of the C-FRP ropes in the joint of specimen JC0F2X2C. Further, in high SDs (> 2%), the abovementioned condition is verified since the mounted C-FRP ropes maintained the joint body intact at these loading steps and efficiently decreased the shear deformation. The joint shear deformation versus SD curves of specimen JC0 presented in figure 11 show that the highest shear deformations are achieved in the 4th and 5th loading step with SD = 1.5% and 2%, respectively. Considering that there is a high difference with the shear deformation of the previous step, it is deduced that significant damage occurred at these steps.

Damage diagnosis based on commonly used indices

The acquired Voltage response measurements were recorded through the custom-made device and displayed in curves in terms of the frequency range. Each curve depicts the output data of the PZT at the end of each loading step at the release condition of the specimen. Figures 12 and 13 present typical Voltage curves of the PZT1 for both specimens.

In BCJ JC0, three PZT transducers were epoxy-bonded on the concrete surface in the diagonal direction of the

joint body panel (see also Figure 5). Damage diagnosis based on the implementation of the epoxy-bonded PZT patches was addressed through the application of statistical indices RMSD and MAPD. Figures 14 and 15 present the diagrams of RMSD and MAPD values indices of specimen JC0, respectively.

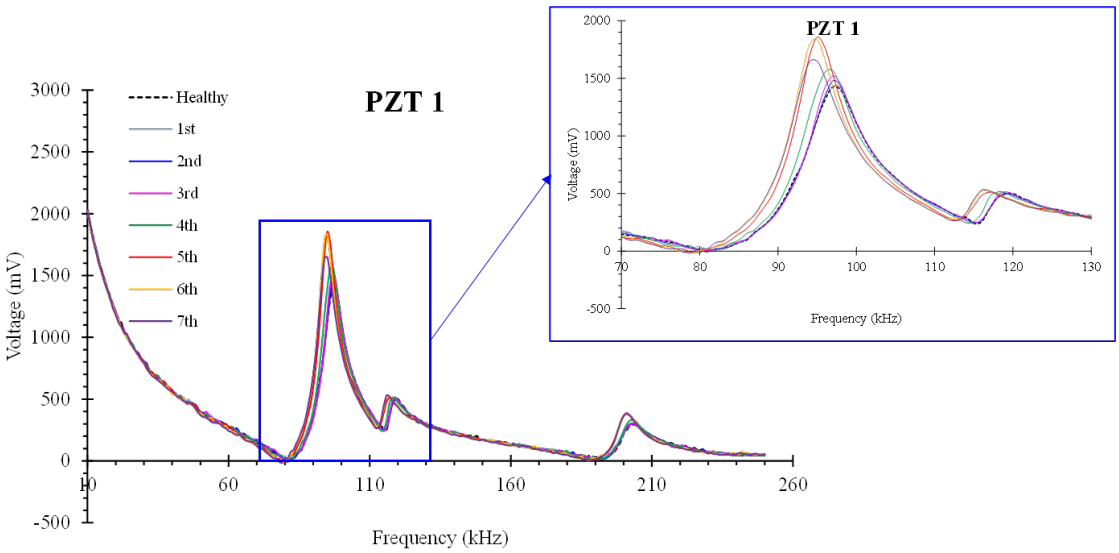

Figure 12. Typical Voltage curves of the PZT1 for all loading steps from the JC0 specimen

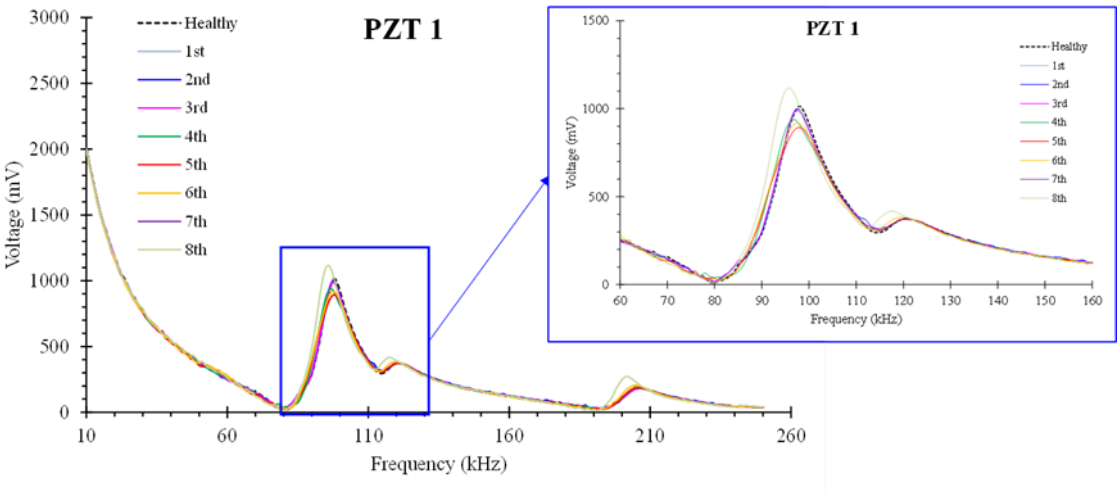

Figure 13. Typical Voltage curves of the PZT1 for all loading steps from the JC0F2X2C specimen

PZT1 transducer shows a significant increment of its RMSD volume ratio at the 4th loading step, which is owed to the extensive cracking propagation in the vicinity of the patch. At the 5th loading step, the RMSD volume ratio of the PZT1, launches to approximately 20% volume ratio, which depicts an extended cracking that agrees with the abovementioned curves of the dissipated energy and the hysteretic response. Similarly, the MAPD values follow the same pattern for PZT1, with slightly higher values. Further, PZT2 transducer shows a slightly ascending volume ratio value in both RMSD and MAPD indices at the 6th loading step, while after that step, there was a malfunction of the transducer due to the spalling of the concrete where it was bonded. Additionally, PZT3 transducer shows slightly ascending values at loading steps 3rd, 4th, and 5th, while at the 6th loading step, the values of the indices are highly increased. All the PZT transducers performed satisfactorily, efficiently diagnosing the cracking severity around their monitoring contiguity. The efficacy of the transducers was also influenced as the cracking distribution propagated in a very tight net of cracks, with fluctuation in their range and properties.

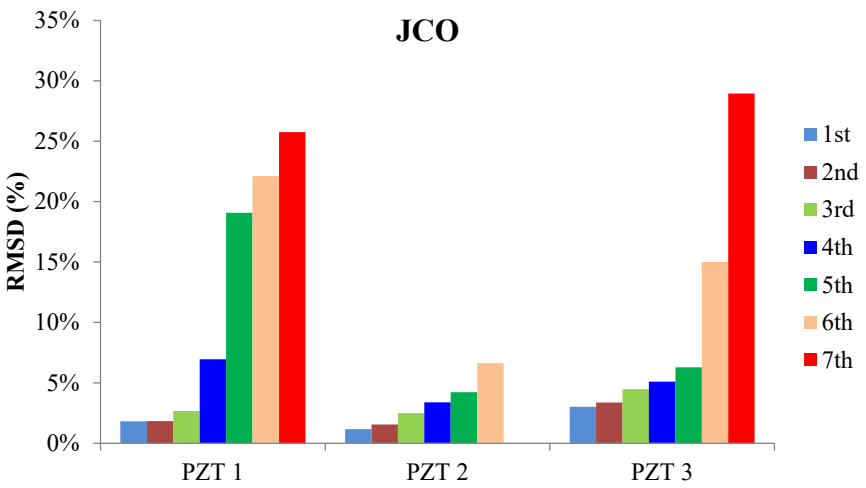

Figure 14. RMSD index values (%) from the JC0 specimen

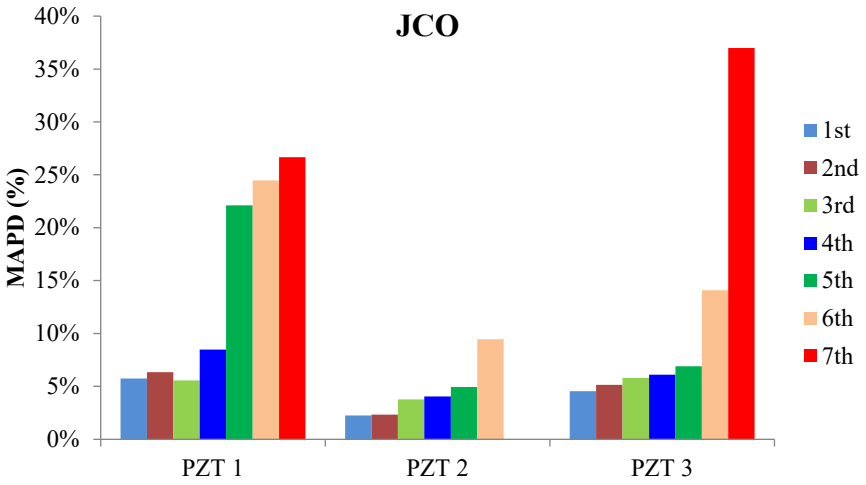

Figure 15. MAPD index values (%) from the JC0 specimen

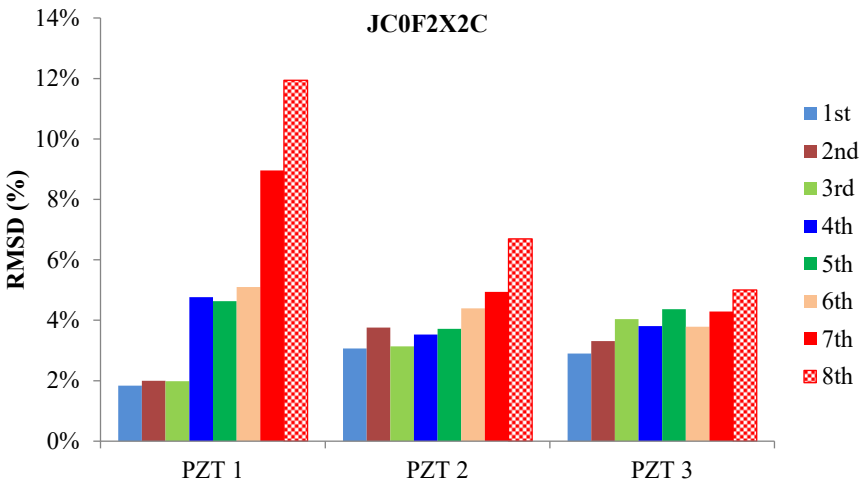

Figure 16. RMSD index values (%) from the JC0F2X2C specimen

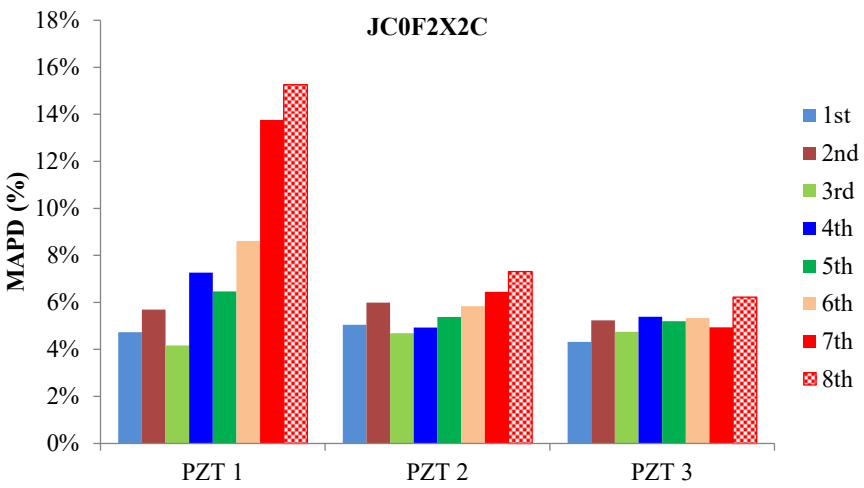

Figure 17. MAPD index values (%) from the JC0F2X2C specimen

In BCJ JC0F2X2C, two PZT transducers were epoxy-bonded on the retrofitting C-FRP ropes to monitor the efficiency of the strengthening technique. Damage diagnosis based on the implementation of the epoxy-bonded PZT patches was addressed by applying statistical indices RMSD and MAPD. Figures 16 and 17 present the diagrams of RMSD and MAPD values indices of specimen JC0F2X2C, respectively.

PZT1 transducer shows a significant increment of its RMSD volume ratio at the 4th loading step, which remains almost stable up to the 6th loading step. The latter is owed to the extensive cracking propagation in the patch's vicinity, the activation, and the contribution of the C-FRP rope to withstand the development of the shear deformations, increasing the resistance of the retrofitted joint. The RMSD volume ratio of PZT1 launches to approximately 9% volume ratio at the 7th loading step, and to 12 % at the 8th cyclic loading step, connoting the stresses development on the rope due to its effort to resist the extended cracking of the joint. The latter agrees with the dissipated energy curves and the specimen's hysteretic response. Similarly, the MAPD values follow the same pattern for PZT1, with slightly higher values at all the cyclic loading steps. This fact also reveals potential excessive damage to the C-FRP rope due to fiber debonding or micro-fracture that has occurred at the mentioned cyclic loading steps.

Further, the PZT2 transducer shows a slightly ascending volume ratio value in both RMSD and MAPD indices from the first to the 5th loading step. In contrast, there is a slight increment of the volume ratios at the 6th and 7th loading steps and a significant increment at the 8th loading state.

In addition, it should be referred that although PZT1 transducer has symmetrically been positioned to PZT2 and mounted to the diagonal C-FRP ropes, the frequency response of PZT1 exhibits differently than the one of PZT1. Nonetheless, the difference can be considerably rationalized by the strain measurements of the column longitudinal steel bar during the cyclic testing procedure. These strains are not symmetrical in both directions, which reveals that the loading cycle with positive (+) direction caused initial tension and more critical damage to the C-FRP rope with PZT1 transducer than the C-FRP rope with PZT2.

Additionally, PZT3 transducer shows minor ascending values at the first, 3rd, and last loading steps. The rope-bonded PZT transducers showed satisfactory performance and efficiently monitored the performance of the strengthening technique following the activation, operation, and contribution of the ropes. The cracking fluctuation in the joint body probably influenced the PZT3 transducer's efficacy, as the distribution of the propagated cracks was limited due to the ropes' operation.

Damage diagnosis based on hierarchical clustering approach

This study also addresses the hierarchical clustering approach (HCA) as a supplementary tool to implement the damage diagnosis process better. The HCA could be performed as a tool for a primary sorting of the acquired data and then proceeding with the statistical analysis using common indices or as a final assisting tool to re- or co-evaluate the extracted indices.

The main reason for implementing HCA in this work was the realization that common indices numerically evaluate the damage level. However, it is often observed that the same damage index values could correspond to different structural conditions, which could easily lead to false alerts. i.e., the loading impact.

The HCA was adopted to be supplementally applied with the quantitative data analysis process, enhancing the attempt to identify more specific properties of the forthcoming or developed damage and clearly distinguish the false alerts inserted by the induced load. In this scope, all measurements of each PZT transducer are evaluated through an unsupervised machine learning method. The extracted results for both specimens are presented in figures 18-23 in a dendrogram format.

The explication of an HCA dendrogram is based on the degree of dissimilarity between the healthy condition measurement and any successive one. In this way, for specimen JC0, for PZT1 transducer, the HCA dendrogram shows an alteration at the 4th cyclic loading, which constitutes an indication of the formation of severe damage near the vicinity of the PZT transducer. Further, there is also a high dissimilarity degree at the following cyclic loading step 5th which indicates either the formation of new severe damage or the expansion of the existing. Moreover, in the HCA dendrogram of PZT2 transducer, there are two alterations at the 5th and 6th loading steps, where the cracking pattern developed near the patch area. Further, regarding the performance of PZT3 transducer, the first change at the 4th loading step was kept stable at the 5th loading step. Then, at the 6th loading state, a high degree of dissimilarity is also presented, indicating the formation of a potential cracking in both cases.

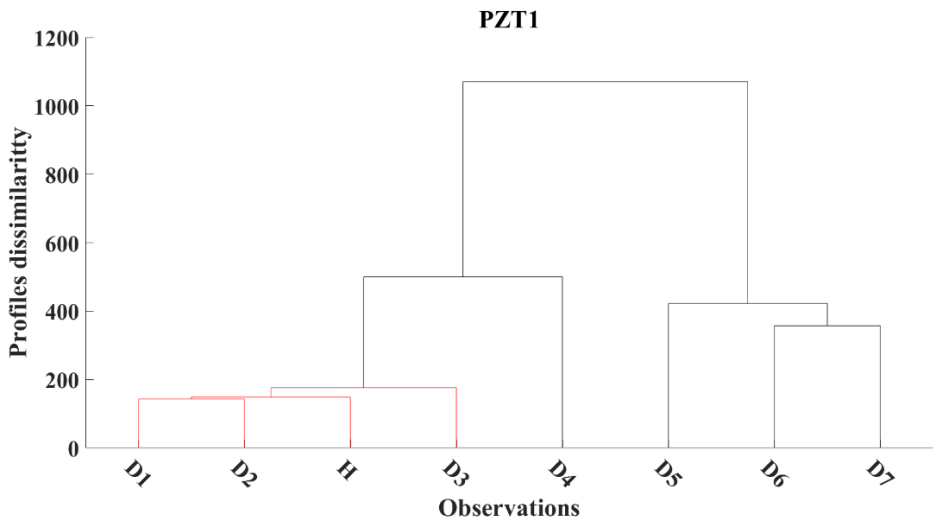

Figure 18. HCA dendrogram of PZT1 for JC0 specimen

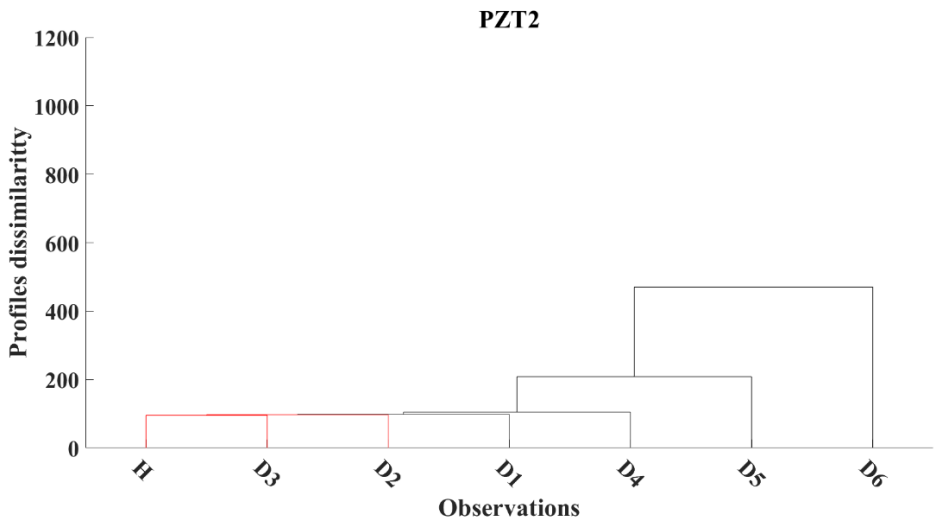

Figure 19. HCA dendrogram of PZT2 for JC0 specimen

Regarding the HCA dendrograms of specimen JC0F2X2C, Figure 21 presents the results of PZT1 transducer. The first altered observation occurred in the 4th cyclic loading state. After that, the subsequent alteration occurred in the 5th and 7th cyclic loading step, whereas the C-FRP ropes were operated under the subjection of the imposed developed stresses. Similarly, for PZT2 transducer, the first alteration occurred in the 4th cyclic loading; after that, at loading steps 6th and 8th presented changes to the HCA dendrogram, which also connotes the operation of the ropes to establish a mechanism of resistance towards the development of shear deformations in the joint body. Figure 22 illustrates the HCA dendrogram values of PZT2 transducer.

Finally, Figure 23 presents the results of the HCA dendrogram of PZT3 transducer. The values indicate a potential damage formation at the 3rd cyclic loading. After that, at the 5th, 6th, and 8th loading steps.

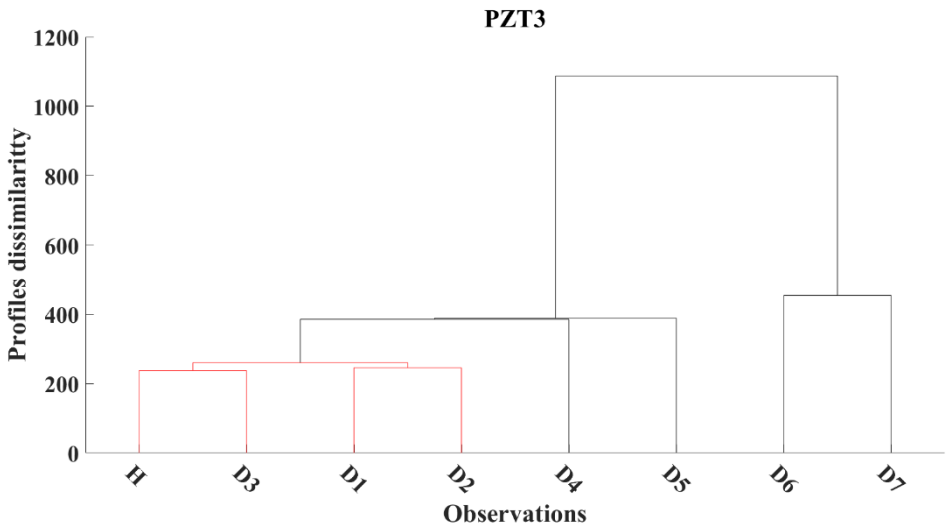

Figure 20. HCA dendrogram of PZT3 for JC0 specimen

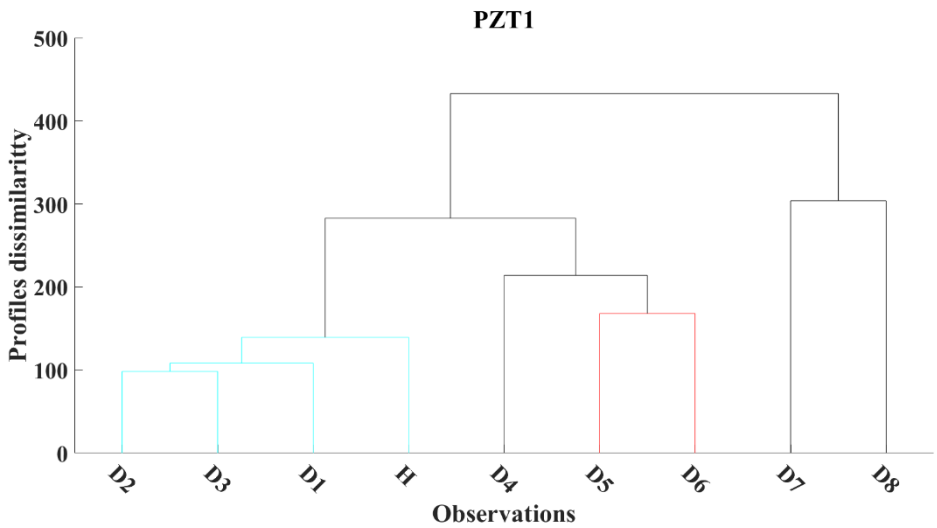

Figure 21. HCA dendrogram of PZT1 for JC0F2X2C specimen

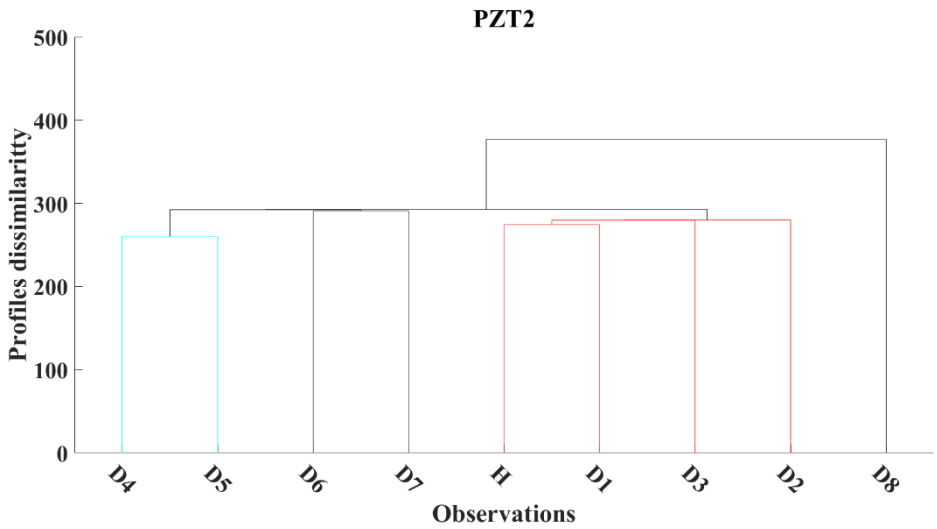

Figure 22. HCA dendrogram of PZT2 for JC0F2X2C specimen

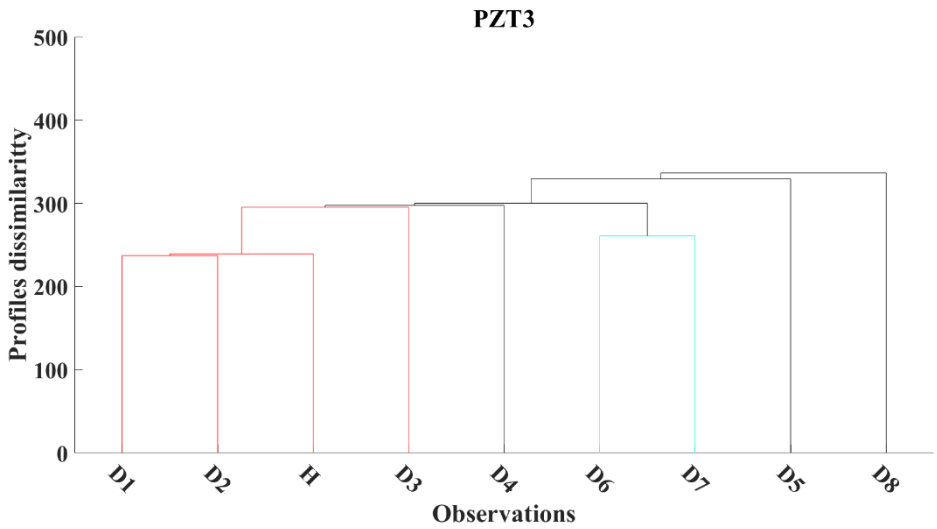

Figure 21. HCA dendrogram of PZT3 for JC0F2X2C specimen

Damage diagnosis based on combining multiple methods

The diagnosis of the damage demands a reliable sequence of parameters. The first step is the applied method of SHM. Further, the instrumentation of the used technique, the data acquisition, and the analysis. In the scope of this study, multiple parameters were evaluated and compared to enhance the reliability of the damage diagnosis method. The extracted observations of the hysteretic response, the dissipated energy curves, the cracking pattern and the performance of the examined BCJ specimens, the acquired data of the followed SHM technique, and the combination or the comparisons among the abovementioned tools could lead to a more precise and accurate process of damage diagnosis. Thus, the damage evaluation of the BCJ specimens can be detected by the imposed load versus the deformation and the cracking propagation of the structural members during the subjected cyclic loading.

Nevertheless, applying the recommended EMA-based PZT-enabled SHM technique provided real-time, continuous, and in-situ measurements for early warning and damage diagnosis of impending failure in real-life RC structures.

The extracted data from the custom-made wireless device through the application of PZT transducers and also following the recommended SHM process and the acquired data using the conventional instrumentation such as LDTs and SLVDTs offers strong indications of damage diagnosis throughout the whole imposed cyclic loading

sequence. However, the proposed EMA-based PZT-enabled SHM technique offers two more benefits. This method can provide (a) remote, continuous non-destructive inspection and reliable damage evaluation and (b) real-time assessment of damage degree with early warning indications of critical failures at initial damage stages.

CONCLUSION

This study investigated the application of a recently developed strengthening technique of RC BCJs and columns using C-FRP ropes. The EMA-based PZT-enabled method of SHM was implemented to evaluate damage diagnosis and the efficiency of the retrofitting technique. Furthermore, the acquired measurements via LDTs and LVDTS enhanced the verification of the evaluation process. Some essential results are gleaned from the below conclusions:

- EMA-based SHM method and the applied instrumental equipment achieved to diagnose the occurred damages at both specimens at early damage states in a satisfactory response, fulfilling the scope of the prompt diagnosis for providing essential information for crisis response and management.
- The acquired Voltage responses of the externally epoxy-bonded PZT transducers on concrete and the C-FRP ropes were statistically analyzed through RMSD and MAPD indices. The scalar indices' results confirmed the specimens' structural integrity at any loading step for all the PZT transducers;
- The measurements of the shear deformations of the joint body (LVDTs) also verified the results adopted from the PZT transducers; Further, the shear deformations results demonstrated the efficiency of the retrofitting technique exhibiting lower values of deformation.
- The measurements of PZT transducers, LVDTs, and LDTs confirmed the efficacy of the applied strengthening technique using C-FRP ropes;
- The HCA seems to be a beneficial supplementary tool to sort the acquired data and enhance the verification of the damage diagnosis process;
- All the above highlights could advocate the conclusion that the combination of the proposed techniques of retrofitting (with C-FRP ropes) and SHM (EMA-based PZT-enabled) of RC structures fulfill the resilience's demands, assisting in developing resilient societies
- The developed PZT-enabled SHM system should be further implemented in real-life RC applications to investigate the level of efficiency;
- PZT transducer's installation and positioning influence the EMA technique's accuracy and capability. The determination of damage's qualities should be further investigated to improve the performance of damage diagnosis.

ACKNOWLEDGMENTS

The authors also acknowledge support of this work by the project "Risk and Resilience Assessment Center—Prefecture of East Macedonia and Thrace-Greece." (MIS 5047293) which is implemented under the Action "Reinforcement of the Research and Innovation Infrastructure", funded by the Operational Programme "Competitiveness, Entrepreneurship and Innovation" (NSRF 2014–2020) and co-financed by Greece and the European Union (European Regional Development Fund).

REFERENCES

Abdelgawad, A.A., Gonzalez, J.J. (2019). Reliability of expert estimates of cascading failures in Critical Infrastructure. *Proceedings of the 16th ISCRAM Conference – València, Spain, May 2019*. https://iscram2019.webs.upv.es/wp-content/uploads/2019/09/ISCRAM2019_Proceedings.pdf

Chalioris, C. E., Papadopoulos, N. A., Angeli, G. M., Karayannis, C. G., Liolios, A. A., and Providakis, C. P. (2015). Damage Evaluation in Shear-Critical Reinforced Concrete Beam using Piezoelectric Transducers as Smart Aggregates. *Open Engineering*, *5*(1). https://doi.org/10.1515/eng-2015-0046

Chalioris, C., Kosmidou, P.-M., and Papadopoulos, N. (2018). Investigation of a New Strengthening Technique for RC Deep Beams Using Carbon FRP Ropes as Transverse Reinforcements. *Fibers*, *6*(3), 52. https://doi.org/10.3390/fib6030052

Chen, H., Xu, B., Zhou, T., and Mo, Y.-L. (2019). Debonding detection for rectangular CFST using surface wave measurement: Test and multi-physical fields numerical simulation. *Mechanical Systems and Signal Processing*,

117, 238–254. https://doi.org/10.1016/j.ymssp.2018.07.047

Comes, T., Bertsch, V., and French, S. (2013). Designing Dynamic Stress Tests For Improved Critical Infrastructure Resilience, *Conference Proceedings - 10th International Conference on Information Systems for Crisis Response and Management, ISCRAM 2013* (pp. 1003-1015). (Proceedings of the International ISCRAM Conference; Vol. 2013-May).

Gandhi, R., Linzel, D., Sim, C., Khazanchi, D., & Ricks, B. (2018). The hidden crisis: Developing smart big data pipelines to address grand challenges of bridge infrastructure health in the United States. In B. Tomaszewski, & K. Boersma (Eds.), *Conference Proceedings - 15th International Conference on Information Systems for Crisis Response and Management, ISCRAM 2018* (pp. 1003-1015). (Proceedings of the International ISCRAM Conference; Vol. 2018-May). Information Systems for Crisis Response and Management, ISCRAM.

Golias, E., Zapris, A. G., Kytinou, V. K., Kalogeropoulos, G. I., Chalioris, C. E., and Karayannis, C. G. (2021). Effectiveness of the Novel Rehabilitation Method of Seismically Damaged RC Joints Using C-FRP Ropes and Comparison with Widely Applied Method Using C-FRP Sheets—Experimental Investigation. *Sustainability*, *13*(11), 6454. https://doi.org/10.3390/su13116454

Golias, E., Zapris, A. G., Kytinou, V. K., Osman, M., Koumtzis, M., Siapera, D., Chalioris, C. E., and Karayannis, C. G. (2021). Application of X-Shaped CFRP Ropes for Structural Upgrading of Reinforced Concrete Beam–Column Joints under Cyclic Loading–Experimental Study. *Fibers*, *9*(7), 42. https://doi.org/10.3390/fib9070042

Jagadale, U. T., Nayak, C. B., Mankar, A., Thakare, S. B., and Deulkar, W. N. (2020). An experimental-based python programming for structural health monitoring of non-engineered RC frame. *Innovative Infrastructure Solutions*, *5*(1), 10. https://doi.org/10.1007/s41062-020-0260-x

Jiang, T., Kong, Q., Wang, W., Huo, L., and Song, G. (2016). Monitoring of Grouting Compactness in a Post-Tensioning Tendon Duct Using Piezoceramic Transducers. *Sensors*, *16*(8), 1343. https://doi.org/10.3390/s16081343

Karayannis, C., Golias, E., and Kalogeropoulos, G. I. (2022). Influence of Carbon Fiber-Reinforced Ropes Applied as External Diagonal Reinforcement on the Shear Deformation of RC Joints. *Fibers*, *10*(3), 28. https://doi.org/10.3390/fib10030028

Karayannis, C. G., Golias, E., Naoum, M. C., and Chalioris, C. E. (2022). Efficacy and Damage Diagnosis of Reinforced Concrete Columns and Joints Strengthened with FRP Ropes Using Piezoelectric Transducers. *Sensors*, *22*(21), 8294. https://doi.org/10.3390/s22218294

Karayannis, C. G., and Sirkelis, G. M. (2008). Strengthening and rehabilitation of RC beam–column joints using carbon-FRP jacketing and epoxy resin injection. *Earthquake Engineering & Structural Dynamics*, *37*(5), 769–790. https://doi.org/10.1002/eqe.785

Mishra, Mayank, Kumar, M. Kranti, and Maity, Damodar. (n.d.). *Experimental evaluation of the behaviour of bamboo-reinforced beam–column joints*. https://doi.org/10.1007/s41062-019-0237-9

Perera, R., Torres, L., Ruiz, A., Barris, C., and Baena, M. (2019). An EMI-Based Clustering for Structural Health Monitoring of NSM FRP Strengthening Systems. *Sensors*, *19*(17), 3775. https://doi.org/10.3390/s19173775

Pham, Q.-Q., Dang, N.-L., and Kim, J.-T. (2021). Smart PZT-Embedded Sensors for Impedance Monitoring in Prestressed Concrete Anchorage. *Sensors*, *21*(23), 7918. https://doi.org/10.3390/s21237918

Psathas, A.P., Iliadis, L., Achillopoulou, D.V., Papaleonidas, A., Stamataki, N.K., Bountas, D., and Dokas, I.M. (2022). Autoregressive Deep Learning Models for Bridge Strain Prediction. Engineering Applications of Neural Networks, 23rd International Conference, EAAAI/EANN 2022 Chersonissos, Crete, Greece, June 17–20, 2022 Proceedings. https://doi.org/10.1007/978-3-031-08223-8_13

Santarsiero, G., Mishra, M., Singh, M. K., and Masi, A. (2021). Structural health monitoring of exterior beam–column subassemblies through detailed numerical modelling and using various machine learning techniques. *Machine Learning with Applications*, *6*, 100190. https://doi.org/10.1016/j.mlwa.2021.100190

Sevillano, E., Sun, R., Gil, A., and Perera, R. (2016). Interfacial crack-induced debonding identification in FRP-strengthened RC beams from PZT signatures using hierarchical clustering analysis. *Composites Part B: Engineering*, *87*, 322–335. https://doi.org/10.1016/j.compositesb.2015.09.006

Singh, S., Sharma, S., and Kwatra, N. (2021). Damage progression in RC BEAM-COLUMN joints under cyclic

loading using acoustic emission technique. *Structural Concrete*, *22*(6), 3556–3573. https://doi.org/10.1002/suco.202000713

Tafsirojjaman, T., Fawzia, S., and Thambiratnam, D. P. (2021). Structural behaviour of CFRP strengthened beam-column connections under monotonic and cyclic loading. *Structures*, *33*, 2689–2699. https://doi.org/10.1016/j.istruc.2021.06.028

Tsintotas, K. A., Bampis, L., and Gasteratos, A. (2018). Assigning Visual Words to Places for Loop Closure Detection. *2018 IEEE International Conference on Robotics and Automation (ICRA)*, 1–7. https://doi.org/10.1109/ICRA.2018.8461146

Tsintotas, K. A., Sevetlidis, V., Papapetros, I. T., Balaska, V., Psomoulis, A., & Gasteratos, A. (2022). BK tree indexing for active vision-based loop-closure detection in autonomous navigation. *2022 30th Mediterranean Conference on Control and Automation (MED)*, 532–537. https://doi.org/10.1109/MED54222.2022.9837138

Tsonos, A. G. (2009). *Ultra-high-performance fiber reinforced concrete: An innovative solution for strengthening old R/C structures and for improving the FRP strengthening method*. 273–284. https://doi.org/10.2495/MC090261

Tsonos A. G. (2014). An innovative solution for strengthening of old R/C structures and for improving the FRP strengthening method. *Structural Monitoring and Maintenance*, *1*(3), 323–338. https://doi.org/10.12989/SMM.2014.1.3.323

Tsonos A. G. (2019). Model for the evaluation of the beam-column joint ultimate strength -a more simplified version. *Earthquakes and Structures*, *16*(2), 141–148. https://doi.org/10.12989/EAS.2019.16.2.141

Valença, J., and Carmo, R. N. F. (2017). Method for assessing beam column joints in RC structures using photogrammetric computer vision. *Structural Control and Health Monitoring*, *24*(11), e2013. https://doi.org/10.1002/stc.2013

Voutetaki, M. E., Naoum, M. C., Papadopoulos, N. A., and Chalioris, C. E. (2022). Cracking Diagnosis in Fiber-Reinforced Concrete with Synthetic Fibers Using Piezoelectric Transducers. *Fibers*, *10*(1), 5. https://doi.org/10.3390/fib10010005

Voutetaki, M. E., Naoum, M. C., Papadopoulos, N. A., Sapidis, G., and Chalioris, C. E. (2021). Cracking Diagnosis in Fibre Reinforced Concrete Cubes and Cylinders with Synthetic Fibres using a PZT-based Health Monitoring System. *Scholars Journal of Engineering and Technology*, *9*(9), 140–151. https://doi.org/10.36347/sjet.2021.v09i09.004

Voutetaki, M. E., Papadopoulos, N. A., Angeli, G. M., and Providakis, C. P. (2016). Investigation of a new experimental method for damage assessment of RC beams failing in shear using piezoelectric transducers. *Engineering Structures*, *114*, 226–240. https://doi.org/10.1016/j.engstruct.2016.02.014

Wang, C., Xiao, J., Liu, W., and Ma, Z. (2022). Unloading and reloading stress-strain relationship of recycled aggregate concrete reinforced with steel/polypropylene fibers under uniaxial low-cycle loadings. *Cement and Concrete Composites*, *131*, 104597. https://doi.org/10.1016/j.cemconcomp.2022.104597

Wang, C., Zhang, Y., Ma, Z., and Wang, D. (2022). Hysteretic deteriorating behaviors of fiber-reinforced recycled aggregate concrete composites subjected to cyclic compressive loadings. *Journal of Building Engineering*, *49*, 104087. https://doi.org/10.1016/j.jobe.2022.104087

Yan, S., Sun, W., Song, G., Gu, H., Huo, L.-S., Liu, B., and Zhang, Y.-G. (2009). Health monitoring of reinforced concrete shear walls using smart aggregates. *Smart Materials and Structures*, *18*(4), 047001. https://doi.org/10.1088/0964-1726/18/4/047001

Zapris, A. G., Naoum, M. C., Kytinou, V. K., Sapidis, G. M., and Chalioris, C. E. (2023). Fiber Reinforced Polymer Debonding Failure Identification Using Smart Materials in Strengthened T-Shaped Reinforced Concrete Beams. *Polymers*, *15*(2), 278. https://doi.org/10.3390/polym15020278

Zhang, X., Zhang, L., Liu, L., and Huo, L. (2018). Prestress Monitoring of a Steel Strand in an Anchorage Connection Using Piezoceramic Transducers and Time Reversal Method. *Sensors*, *18*(11), 4018. https://doi.org/10.3390/s18114018